Interfacial characterisation of multi-material 316L stainless steel/Inconel 718 fabricated by laser powder bed fusion

Shahir Mohd Yusuf[a], Xiao Zhao[a], Shoufeng Yang[a,b], and Nong Gao[a,*]

[a]Materials Research Group, Faculty of Engineering and Physical Sciences, University of Southampton, Southampton SO17 1BJ, UK

[b]Production Engineering, Machine Design and Automation Section, Department of Mechanical Engineering, Katholieke Universiteit Leuven (KU Leuven), Leuven 3001, Belgium

ABSTRACT

In this study, the interfacial region of multi-material 316L stainless steel/Inconel 718 (316L SS/IN718) fabricated by laser powder bed fusion (L-PBF) is investigated in detail for the first time. The interfacial region consists of a fusion zone (FZ) with intermixed fused Fe and Ni, and individual 316L SS and IN 718 regions. Solid metallurgical bonding is achieved, as evidenced by the low porosity level (~0.27%) and absence of cracks. Microhardness measurements show an average of ~265 HV at the interfacial region, and ~304 HV and ~223 HV at the individual IN 718 and 316L SS regions, respectively.

Keywords: interface; multi-material; additive manufacturing; laser powder bed fusion; structural; diffusion

* Corresponding author.

E-mail addresses: symy1g12@soton.ac.uk (S. Mohd Yusuf), xiao.zhao@soton.ac.uk (X. Zhao), shoufeng.yang@kuleuven.be (S. Yang), n.gao@soton.ac.uk (N. Gao).

1. Introduction

The microstructures of additive manufacturing (AM) of individual 316L SS and IN 718, respectively via laser- powder bed fusion (L-PBF) normally include: (i) cellular sub-structures, (ii) equiaxed and columnar grains, and (iii) fine precipitates in some cases, e.g. Cr-based spherical nano-silicates in 316L SS, as well as laves phase, γ"-Ni_3Nb, and δ-Ni_3Nb (if subjected to heat treatment) in IN 718 [1–3]. Altogether, these microstructures contribute to the comparable or even superior strength of these two AM materials compared to their conventionally manufactured (CM) counterparts [4]. So far, research on the L-PBF of 316L

SS/IN 718 combination are still limited [5,6], thus the microstructural characteristics and properties of the bonding interface are not well understood. Therefore, the present study is the first to elucidate the interfacial characterisation of 316L SS/IN 718 fabricated by L-PBF AM technique, via extensive microscopy analysis and Vickers microhardness (HV) tests.

2. Materials and methods

Two small blocks of alternating materials (316L SS and IN 718) with dimensions of 10×10×5 mm were built successively to produce a single rectangular bar of 10×10×50 mm using a novel multi-material L-PBF machine equipped with multiple powder deposition mechanism and cleaning system, developed at the University of Southampton. A single set of processing parameters were used for both materials: Laser power (L): 300 W, scan speed (P): 900 mm s^{-1}, layer thickness (d): 30 µm, and scan line spacing (h): 80 µm. A uni-directional scan strategy, rotated by 90° between each layer was used, and the build chamber was initially purged with argon gas. The smaller blocks were built vertically upwards on a 304L SS substrate, parallel to the z-direction as shown in Fig. 1. Microstructural observations were then conducted at the interface between two different materials using Olympus BX-51 optical microscope (OM) and JSM-JEOL 6500 FEI scanning electron microscope (SEM) facility, following normal sample preparation steps. The porosity content for the whole specimen were evaluated via ImageJ software analysis of polished OM images through typical binarisation and thresholding procedures. In addition, electron backscattered diffraction (EBSD) analysis was also carried out to characterise the grain size and morphology at the interfacial region in more detail by electropolishing the polished specimens in 80% methanol and 20% perchloric acid at 16 V and 0.5 A for 18 s. EBSD images were taken at the interfacial region within 100×100 µm areas and step size of 0.1 µm covering ~100 grains each. HV measurements (load: 100 gf, dwell time: 15 s) were carried out by carefully selecting 50 locations at the interfacial region, and at each individual material regions.

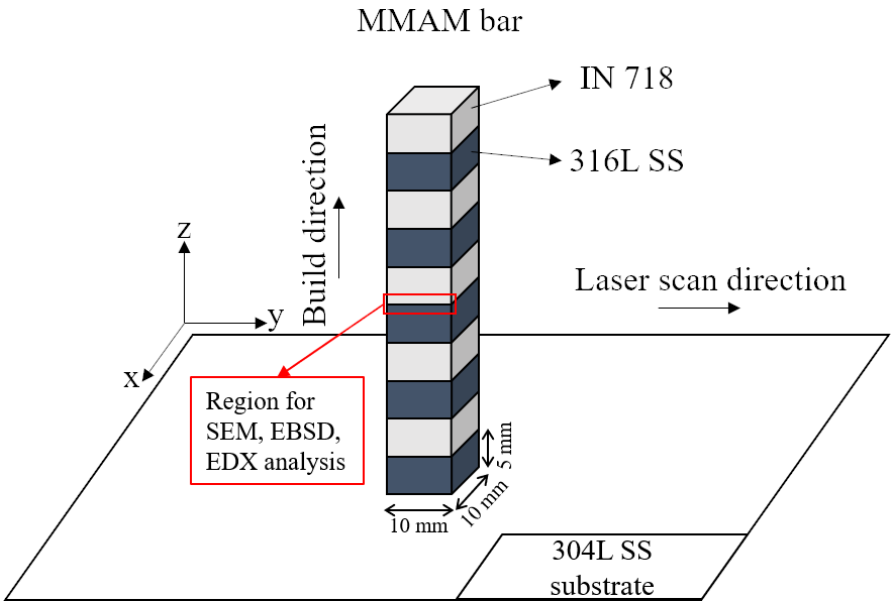

Fig. 1 Complete build schematic and location for microstructural characterisation (red).

3. Results and discussion

Fig. 2 displays the interfacial microstructures of SLM-fabricated 316L SS/IN 718 which can be divided into three sections: IN 718 region, fusion zone (FZ), and 316L SS region. With an estimated width of ~100 µm, the FZ consists of an intermixed region rich with Fe and Ni as illustrated by the electron dispersive x-ray spectroscopy (EDX) images in Figs. 2(a) and (b). Upon consideration of the 30 µm layer thickness in this study, this suggests significant dilution and diffusion of the matrix element of both materials across 3 – 4 layers of deposited powder bed at the interfacial region [7–9]. No cracks are observed, but some irregular-shaped lack-of-fusion pores are apparent within the FZ (circled areas in Figs. 2(a) and (b)). Nevertheless, the porosity content at the interfacial region is only 0.27% compared to 0.81% of the overall solidified part as measured via ImageJ analysis software. Altogether, these indicate good metallurgical bonding has been achieved at the interface, which might also be contributed by the compatibility of both materials that have a similar γ-FCC lattice structure, thus interacting well to melt and fuse together upon interaction with the laser heat source [10,11].

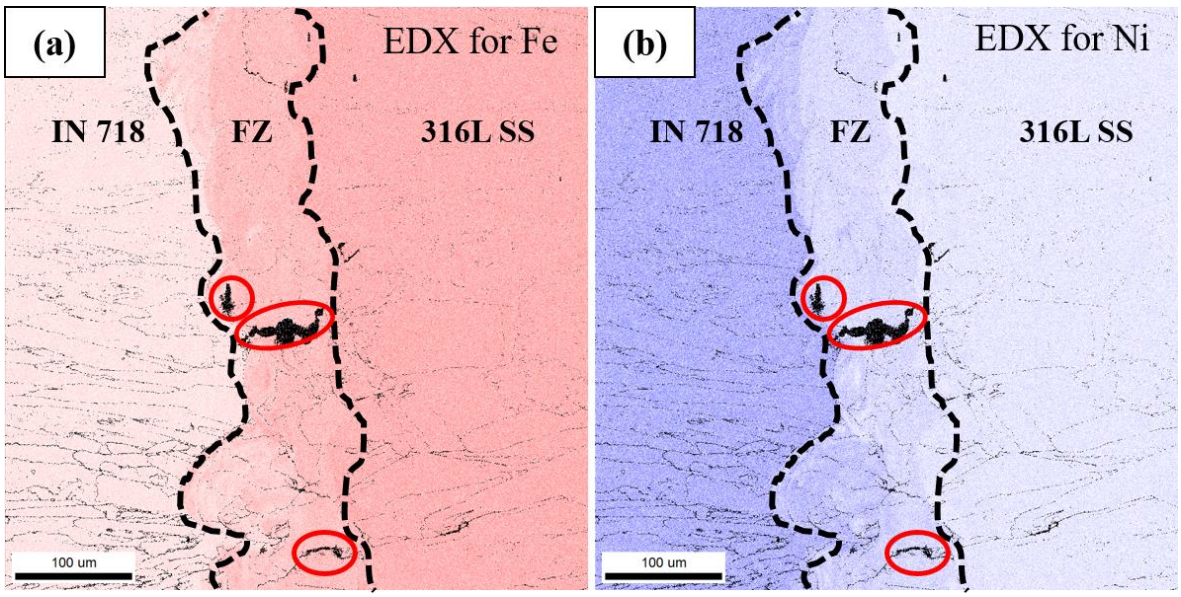

Fig. 2 EDX map for (a) Fe and (b) Ni taken at the interfacial region.

The EBSD grain orientation map shown in Fig. 3(a) show that the FZ comprises of equiaxed grains (average: 45±3 μm), while the individual IN 718 and 316L SS regions consist of elongated columnar grains averaged at 55±5 μm and 85±3 μm, respectively. The columnar grain morphology of the individual material regions is expected due to the superior thermal gradient along the z-direction compared to the x-y plane, favouring directional solidification and promoting epitaxial growth [12]. The finer columnar grains at the IN 718 region compared to that at the 316L SS region can be correlated to the lower coefficient of thermal expansion (CTE) of IN 718, which restricts the expansion area and volume of the solidified grains within a given temperature gradient. However, the fine, equiaxed grains observed at the FZ can be caused by the combination of sudden material change and high cooling rates of SLM processing, which results in significantly higher thermal gradients that suppress grain growth and recrystallisation [9,13].

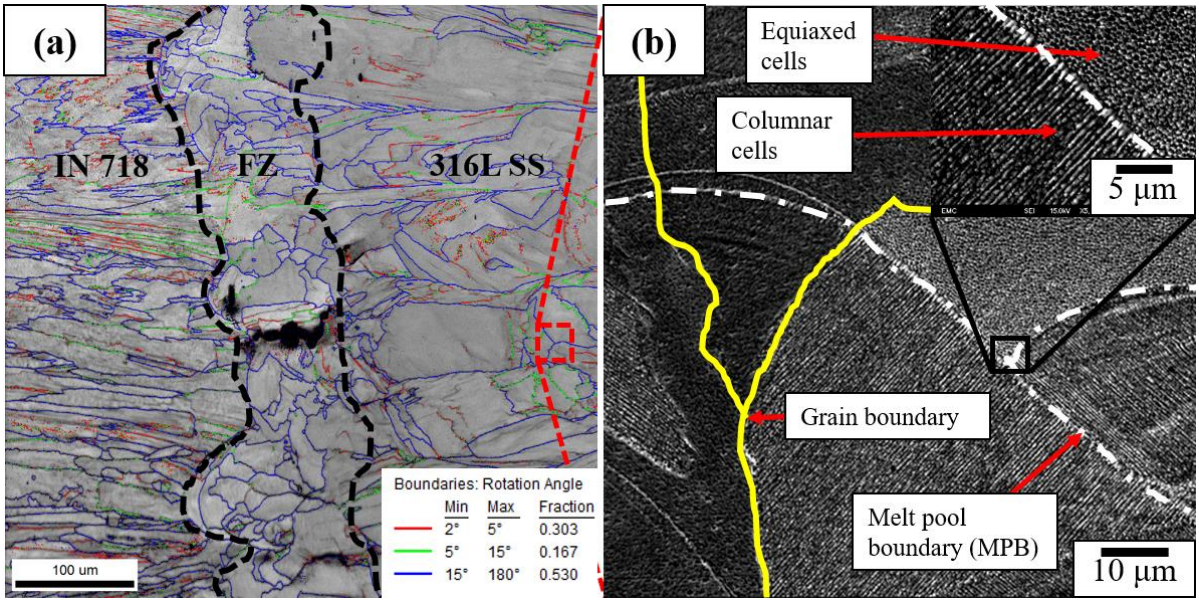

Fig. 3 (a) EBSD grain boundary misorientation map at the interfacial region, (b) SEM image of the highlighted region in (a); cellular sub-structures with LAGBs growing through multiple MPBs within a single grain having a HAGB (inset).

In addition, Fig. 3(a) also reveals the misorientation angles of the grain growth at the interfacial region. It can be observed that most of the grains (~53%) can be categorised as having high-angle grain boundaries (HAGBs), with misorientation angles >15°. This can be ascribed to the high laser beam energy that partially remelts previously solidified layer to fuse with successively melted powder layers, encouraging grain nucleation and recrystallisation to form HAGBs [14]. Contrastingly, the remaining grain boundaries (~47%) are classified as low-angle grain boundaries (LAGBs) having misorientation angles from 2°–15°. In AM materials, such LAGBs are attributed to the dense cellular (columnar or equiaxed) sub-structures that stores dislocations (e.g. Fig. 3(b)), which are formed due to the high internal stress resulting from the rapid heating/solidification cycles [2,15].

In addition, it is apparent from Fig. 3(a) that the IN 718 region possesses higher density of LAGBs compared to the FZ and the 316L SS region, which implies the formation of denser cellular sub-structures here compared to the other two sections [15,16]. This is inferred to be the result of the lower CTE value of IN 718 than that of 316L SS, which not only limits the area and volume expansion of grains, but also hinder nucleation and recrystallisation of grains that are the precursors for the formation of HAGBs.

On the other hand, microhardness measurements at the interfacial region reveal the following average HV values: 304±16 HV (IN 718 region), 265±13 HV (FZ), and 223±11 HV (316L SS region). The higher hardness of the IN 718 region compared to the other two locations can be attributed to the larger fractions of HAGBs and LAGBs due to the finer columnar grains and denser cellular sub-structures as shown in Fig. 2(a). Both types of GBs provide significantly more sites to impede dislocation motions and increase the hardness. Although the FZ possesses high fractions of HAGBs, but the lack of LAGBs (cellular sub-structures) results in lesser locations to restrict dislocation motions that reduces the hardness. Similarly, the coarser elongated grains and lesser LAGBs at the 316L SS region could explain its lowest hardness due to the lack of dislocation motion inhibitor sites.

4. Conclusion

The interfacial region of SLM-fabricated multi-material 316L SS/IN 718 was characterised by extensive SEM/EBSD observations, porosity analysis, and Vickers hardness testing. The results show that the interfacial region consists of the fusion zone (FZ) and individual 316L SS and IN 718 regions. In addition, the low porosity content and absence of cracks suggest sound metallurgical bonding at the interfacial region.he IN 718 region exhibited the highest hardness, compared to the FZ and 316L SS regions, due to the combined large fractions of HAGBs and LAGBs.

Acknowledgements

None.

References

[1] W.M. Tucho, V.H. Lysne, H. Austbø, A. Sjolyst-Kverneland, V. Hansen, Investigation of effects of process parameters on microstructure and hardness of SLM manufactured SS316L, J. Alloys Compd. 740 (2018) 910–925.

[2] W.M. Tucho, P. Cuvillier, A. Sjolyst-Kverneland, V. Hansen, Microstructure and hardness studies of Inconel 718 manufactured by selective laser melting before and after solution heat treatment, Mater. Sci. Eng. A. 689 (2017) 220–232.

[3] K.N. Amato, S.M. Gaytan, L.E. Murr, E. Martinez, P.W. Shindo, J. Hernandez, S. Collins, F. Medina, Microstructures and mechanical behavior of Inconel 718 fabricated by selective laser melting, Acta Mater. 60 (2012) 2229–2239.

[4] S. Gorsse, C. Hutchinson, M. Gouné, R. Banerjee, Additive manufacturing of metals: a brief review of the characteristic microstructures and properties of steels, Ti-6Al-4V and high-entropy alloys, Sci. Technol. Adv. Mater. 18 (2017) 584–610.

[5] C. Wei, L. Li, X. Zhang, Y.H. Chueh, 3D printing of multiple metallic materials via modified selective

laser melting, CIRP Ann. 67 (2018) 245–248.
[6] C. Wei, Multiple Material Selective Laser Melting: A New Approach, Laser User. (2018) 18–19.
[7] J. Chen, Y. Yang, C. Song, M. Zhang, S. Wu, D. Wang, Interfacial microstructure and mechanical properties of 316L /CuSn10 multi-material bimetallic structure fabricated by selective laser melting, Mater. Sci. Eng. A. 752 (2019) 75–85.
[8] S.L. Sing, L.P. Lam, D.Q. Zhang, Z.H. Liu, C.K. Chua, Interfacial characterization of SLM parts in multi-material processing: Intermetallic phase formation between AlSi10Mg and C18400 copper alloy, Mater. Charact. 107 (2015) 220–227.
[9] Z.H. Liu, D.Q. Zhang, S.L. Sing, C.K. Chua, L.E. Loh, Interfacial characterization of SLM parts in multi-material processing: Metallurgical diffusion between 316L stainless steel and C18400 copper alloy, Mater. Charact. 94 (2014) 116–125.
[10] A. Hinojos, J. Mireles, A. Reichardt, P. Frigola, P. Hosemann, L.E. Murr, R.B. Wicker, Joining of Inconel 718 and 316 Stainless Steel using electron beam melting additive manufacturing technology, Mater. Des. 94 (2016) 17–27.
[11] K. Shah, I.U. Haq, A. Khan, S.A. Shah, M. Khan, A.J. Pinkerton, Parametric study of development of Inconel-steel functionally graded materials by laser direct metal deposition, Mater. Des. 54 (2014) 531–538.
[12] V.A. Popovich, E. V. Borisov, A.A. Popovich, V.S. Sufiiarov, D. V. Masaylo, L. Alzina, Functionally graded Inconel 718 processed by additive manufacturing: Crystallographic texture, anisotropy of microstructure and mechanical properties, Mater. Des. 114 (2017) 441–449.
[13] A. Reichardt, R.P. Dillon, J.P. Borgonia, A.A. Shapiro, B.W. McEnerney, T. Momose, P. Hosemann, Development and characterization of Ti-6Al-4V to 304L stainless steel gradient components fabricated with laser deposition additive manufacturing, Mater. Des. 104 (2016) 404–413.
[14] B. AlMangour, D. Grzesiak, J.-M. Yang, Scanning strategies for texture and anisotropy tailoring during selective laser melting of TiC/316L stainless steel nanocomposites, J. Alloys Compd. 728 (2017) 424–435.
[15] X. Liu, C. Zhao, X. Zhou, Z. Shen, W. Liu, Microstructure of selective laser melted AlSi10Mg alloy, Mater. Des. 168 (2019) 1–9.
[16] J.H. Rao, Y. Zhang, X. Fang, Y. Chen, X. Wu, C.H.J. Davies, The origins for tensile properties of selective laser melted aluminium alloy A357, Addit. Manuf. 17 (2017) 113–122.